Effective low-dimensional dynamics of a mean-field coupled network of slow-fast spiking lasers

A. Dolcemascolo,[1] A. Miazek [●],[1] R. Veltz,[2] F. Marino [●],[3] and S. Barland[1]

[1]*Université Côte d'Azur, CNRS, INPHYNI, 1361 Route des Lucioles, 06560 Valbonne, France*
[2]*Inria Sophia Antipolis, MathNeuro Team, 2004 Route des Lucioles - BP93, 06902 Sophia Antipolis, France*
[3]*CNR-Istituto Nazionale di Ottica and INFN, Sez. di Firenze, Via Sansone 1, I-50019 Sesto Fiorentino (FI), Italy*

Low-dimensional dynamics of large networks is the focus of many theoretical works, but controlled laboratory experiments are comparatively very few. Here, we discuss experimental observations on a mean-field coupled network of hundreds of semiconductor lasers, which collectively display effectively low-dimensional mixed mode oscillations and chaotic spiking typical of slow-fast systems. We demonstrate that such a reduced dimensionality originates from the slow-fast nature of the system and of the existence of a critical manifold of the network where most of the dynamics takes place. Experimental measurement of the bifurcation parameter for different network sizes corroborates the theory.

I. INTRODUCTION

The collective dynamics of large networks is a far-reaching research topic and natural examples of reduced dynamics dimensionality abound, like fireflies or applause synchronization [1]. One paradigmatic example is the synchronization of globally coupled phase oscillators as observed in the Kuramoto model [2], whose relative simplicity has allowed tremendous progress (see, e.g., Ref. [3]). Beyond this idealistic case, a particularly relevant situation is that of spiking nodes such as neurons, whose synchronization may play a key role in epilepsy [4]. Thus, many studies focus on the reduced dimensionality of the dynamics of networks of neuron models, see, e.g., [5–11], often enabled by the Ott-Antonsen ansatz [12,13]. In contrast to this rich theoretical literature, controlled experiments are scarce. Here, we study a mean-field coupled network of hundreds of chaotically spiking, dynamically coupled semiconductor lasers. We observe experimentally mixed mode oscillations and chaotic spiking in the mean field. We establish analytically that the effectively observed low-dimensional dynamics results from partial synchronization along the slow manifold of the network, even in absence of synchronization of the fast dynamics of the nodes.

The analysis of optical model systems is often useful in nonlinear science, in particular regarding the synchronization of oscillators as shown in [14,15]. With respect to spiking nodes, optical analogs of neurons abound (recent references include [16–21]) but only very few elements have been experimentally coupled, because each element and coupling must be controlled and accurately tuned into the desired operation regime. Examples so far are limited to self-coupling with delay in [22–24], two nodes in [25–28], and up to six in [29]. In all these cases, the number of elements is small and no attempt of demonstrating reduced dimensionality of the dynamics is done. In contrast, we study a network of 451 elements, two orders of magnitude larger than any previous realization. We establish theoretically the origin of the reduced effective dimensionality experimentally observed and

its validity for arbitrarily large networks. The coupling is dynamic, mimicking *pulse-coupled* networks [30], and the topology can be experimentally tuned from one to all to fully connected. Each of the nodes is a three-dimensional slow-fast system producing relaxation- and mixed mode oscillations and chaotic spiking.

Although the mean field cannot be described by an ordinary differential equation, we observe an effectively low-dimensional dynamics of the network due to the slow-fast nature of the system. Most of the dynamics takes place close to a simple critical manifold whose stability can be computed analytically. The convergence of a bifurcation parameter towards a unique value is observed experimentally by increasing the network size in a quenched disorder configuration.

II. EXPERIMENT

The experiment, shown in Fig. 1(a), is inspired by the chaotic architecture presented in [31,32]. We reproduce it here with a laser array, leading to a mean-field coupled network of many chaotic elements. As shown in [31,32], chaotic spiking arises when a semiconductor laser is driven by an electric signal proportional to the intensity of the light it emits, after a saturable nonlinear transformation and high-pass filtering. This electrical signal constitutes a third, much slower (typically 1 ms) variable, in addition to the light intensity (10 ps) and the semiconductor medium (1 ns).

Here instead of a single laser, an array of 451 vertical cavity surface emitting lasers (VCSELs) is submitted to an AC-coupled nonlinear optoelectronic feedback. All the lasers are driven by a single power supply whose current is distributed evenly between all lasers (we assume identical impedance). The threshold current distribution is symmetric with average value 183.3 mA and standard deviation 5.8 mA. The emitted light is collected by a short focal length lens which forms an image of the array after about 10 cm propagation. Slightly before the image plane, the beam is split in two, for detection and for the optoelectronic reinjection. In this
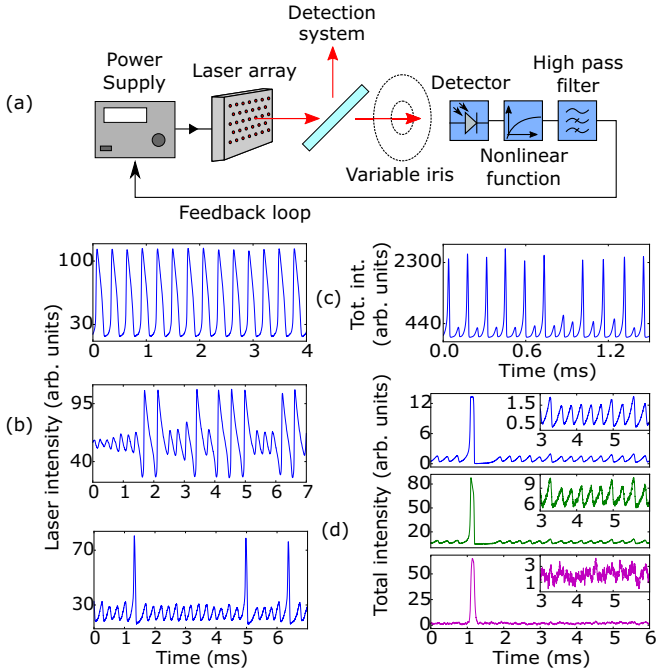
FIG. 1. Experimental setup and typical dynamics. (a) The light emitted by a VCSEL array is converted to an electrical signal which, after filtering and nonlinear transformation, is reinjected into the single current source driving all lasers. (b) Single-laser time traces showing periodic oscillations, chaotic bursting, and spiking (pumping currents 195.0, 196.5, and 187.0 mA). (c) Mean-field time trace of 451 lasers (182.1 mA), showing MMOs. (d) Top panel: total intensity of all 451 lasers, middle and bottom panels: intensity of two different lasers (pumping is 189.9 mA).
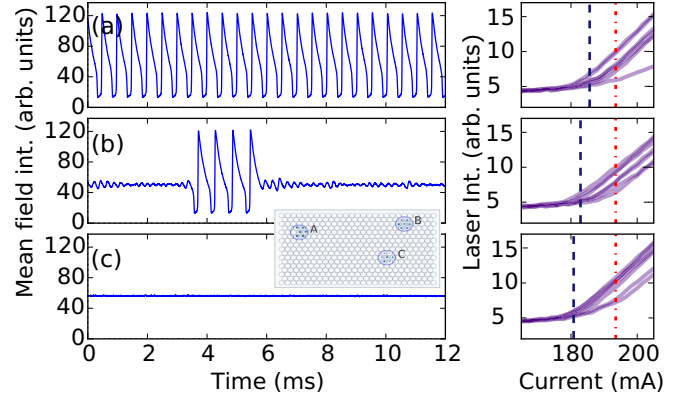

FIG. 2. Dynamics of small networks. Different subpopulations examples [(a), (b) and (c)] show different dynamics (left). Each uncoupled population has a different laser threshold distribution (right), and the black dashed line shows $\langle I_{th} \rangle$ for each population [(a) 185.63 mA, (b) 182.88 mA, (c) 180.81 mA]. Red dash-dotted line: current value used in all measurements (193.50 mA).

beam, at the image plane a variable-aperture iris controls the subpopulation driving the dynamics. The light emitted by this population is converted by a photodetector into a voltage which is logarithmically amplified,[1] providing a saturable nonlinearity. The continuous component is actively filtered out (cutoff frequency 380 Hz), and the resulting signal is sent as a control voltage into the laser power supply, whose input bandwidth is 0–100 kHz. The aperture of the iris controls the coupling, from one to all to globally coupled. Due to the large pitch between the lasers there is no nearest-neighbor coupling. The wavelength distribution of the lasers spans 2 nm and prevents coherent interactions (a far field image is shown in Appendix A). The control parameters are the driving current and the amount of light sent to the detector (controlled via a neutral density filter).

When the iris is closed to select a single laser, this device's intensity drives the current applied to the whole population. The intensity of that particular laser can display complex dynamics, including relaxation oscillations and chaotic bursting or spiking, as shown in Fig. 1(b). When the iris is completely open, the total intensity drives the power supply pumping the whole array, resulting in a mean-field coupled network of 451 nodes. Strikingly, the network can display periodic and chaotic mixed mode oscillations (MMOs) as shown in

Fig. 1(c). In Fig. 1(d) we show synchronous measurements of the total intensity and of the intensity emitted by two different lasers in the mean-field coupled configuration during chaotic spiking: both lasers spike when the network spikes, but only one laser (central trace) displays the subthreshold oscillations observed at the network level (top trace). The other laser remains quiet (at the detection noise level, bottom trace). In most of the explored parameter regimes, nearly all lasers also display the subthreshold oscillations.

Smaller networks can be studied by partly closing the iris and detecting the corresponding population. Different dynamics are observed depending on the subpopulation (Fig. 2). All parameters are constant and the amount of light sent to the detector is scaled with the neutral density filter to maintain the coupling constant when changing population. We show three example subpopulations, A, B, and C, each consisting of seven elements with different threshold current distributions. Network A shows relaxation oscillations, B shows chaotic bursting, and C is stationary. Other examples can be found, but in all cases the dynamics of the total intensity seems low dimensional. The existence of a well-identified low-dimensional dynamics in populations of identical size but with distinct average threshold suggests that this parameter controls the dynamics.

III. MODEL

The effectively low-dimensional dynamics of this very high dimensional system can be understood from the following theoretical analysis. We consider a population of N semiconductor lasers coupled through a common AC-coupled optoelectronic feedback. Each laser is modeled by rate equations describing the evolution of the optical intensity, carriers, and feedback current. After proper scaling (see Appendix B), the equations read

$$\dot{x}_i = x_i(y_i - 1), \tag{1}$$

$$\dot{y}_i = \gamma[\delta_i - y_i + k(w + f(X)) - x_i y_i], \tag{2}$$

$$\dot{w} = -\epsilon(w + f(X)), \tag{3}$$

---

[1]Based on a diode in the feedback loop of an inverting amplifier.

where time has been normalized to the photon lifetime, x_i, y_i are respectively the dimensionless photon and carrier density of the laser i, and $X = \frac{1}{N}\sum_{i=1}^{N} x_i$ is the total intensity normalized to the number of elements. The global variable w is the (scaled) high-pass filtered feedback current, which includes a saturable nonlinear function $f(X) = A\ln(1 + \alpha X)$. The optical and electrical propagation delays are negligible. All the lasers are considered identical, except for the coherent emission threshold current that is included in the control parameter δ_i (proportional to the ratio between the common pump and the threshold current of each laser).

Since ε is small, we know from the geometric singular perturbation theory [33,34] that where the critical manifold (found by setting $\varepsilon = 0$) is stable, the system will asymptotically converge to it. Thus, the stability of the critical manifold is key to understanding the dynamics of this system. First we analyze a single node, and next we compute the stability of the critical manifold of the network. From that, we establish analytically that the network, as a whole, undergoes very similar slow dynamics to that of a single node, even when the fast dynamics of the nodes is not synchronized.

For $N = 1$, the model is similar to [31,32,35], where MMOs result from the three-dimensional slow-fast dynamics near the fold of a one-dimensional critical manifold. Since the normalized carrier rate γ and AC feedback cutoff frequency ϵ are such that $\epsilon \ll \gamma \ll 1$, Eqs. (1)–(3) are a slow-fast system with three timescales. The slow dynamics takes place near a one-dimensional manifold $\Sigma = \Sigma_x \cup \Sigma_y$. The lower attractive branch Σ_x is given by the zero-intensity solution (the laser is off) $\{x = 0, y_w = \delta_1 + k_1 w, w\}$, while the middle repulsive and upper attracting branch, $\Sigma_y = \{x_w, y = 1, w\}$, are implicitly defined by the equation $\delta_1 - 1 + k_1 w + k_1 f(x_w) - x_w = 0$.

In correspondence with the laser threshold $\delta_0 = 1$, the system undergoes a transcritical bifurcation where the zero-intensity solution $(0, \delta_0, 0)$ and the lasing solution $[\delta_0 - 1, 1, -f(\delta_0 - 1)]$ become unstable and stable, respectively. By further increasing the parameter δ_0, even the stationary lasing solution loses stability through a supercritical Hopf bifurcation, followed by a period doubling cascade and by the abrupt transition to a large-amplitude relaxation orbit. The blowup of such slow-fast phase-space orbits and the occurrence of MMOs can be inferred from the following. We first notice that since w typically changes at a much slower rate than x_0 and y_0, the motion splits into fast and slow epochs. The slow dynamics take place on a one-dimensional manifold $\Sigma = \Sigma_x \cup \Sigma_y$, where the lower attractive branch Σ_x is given by the zero-intensity solution $\{x = 0, y_w = \delta_0 + kw, w\}$ while the middle repulsive and upper attracting branches, $\Sigma_y = \{x_w, y = 1, w\}$, are implicitly defined by the equation $\delta_0 - 1 + kw + kf(x_w) - x_w = 0$. Since two branches rapidly attract all neighboring trajectories while the middle branch repels them, canard and relaxation cycles arise. These features are commonly found even in planar slow-fast systems, but here the presence of a third intermediate timescale, $1/\gamma$, induces more complex scenarios. First of all, the fixed points of the two-dimensional fast subsystem (see Figs. 1 and 2) laying on the upper attractive branch consists of stable foci. As such, the trajectories near these branches consist of shrinking helicoids (see Fig. 3), in contrast with the monotonic decay that
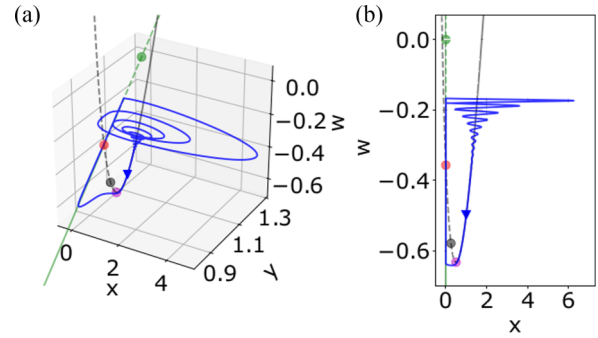

FIG. 3. Numerical simulation of a single laser modeled by Eq. (1) with $N = 1$. The black and the green curve are the two branches of the critical manifold (unstable when dashed). The green and black points are attracting on the manifold they belong to. The magenta point is the minimum of the parabolic part of the critical manifold, where its stability changes. The red point is the (unstable) intersection of the two critical manifolds: $\alpha = 2, k = 0.7, \gamma = 4.0\,10^{-3}, \varepsilon = 10^{-4}, A = 1, \delta_0 = 1.25$. (a) 3D phase space, and (b) projection in the (x, w) plane shows the semiconductor laser relaxation oscillations.

can uniquely be expected in the planar case. Second, a regime of either regular or chaotic MMOs takes place, where canard orbits are separated by small-amplitude, quasiharmonic oscillations surrounding the steady state of the system. When laying on the middle repelling branch, such equilibrium is a saddle focus and trajectories can rotate several times around it before switching to the other stable branch of the manifold. The number of these rotations, as well as the periodic or erratic nature of MMOs, are determined by the rates at which both y_0 and w vary in the vicinity of the saddle focus. This is related to the values of γ and ϵ, but also critically depends on the bifurcation parameter δ_0. This dependence is more and more critical when γ and ϵ differ by orders of magnitude, with chaos becoming increasingly difficult to observe (we observed it up to $\gamma = 4 \times 10^{-3}, \epsilon = 5 \times 10^{-5}$) due to the flattening of the trajectories in the plane transverse to the critical manifold.

When $N > 1$, Figs. 1–3 describe a network of N such elements, globally coupled through their slowest variable w. Defining the mean carrier density $Y = \frac{1}{N}\sum_{i=1}^{N} y_i$, we derive the following rate equations for the coupled network:

$$\dot{X} = -X + \frac{1}{N}\sum_{i=1}^{N} x_i y_i, \tag{4}$$

$$\dot{Y} = \gamma\left[\Delta - Y + k(w + f(X)) - \frac{1}{N}\sum_{i=1}^{N} x_i y_i\right], \tag{5}$$

$$\dot{w} = -\epsilon(w + f(X)), \tag{6}$$

where $\Delta = \frac{1}{N}\sum_{i=1}^{N} \delta_i$. As for $N = 1$, this is a slow-fast system, and much insight can be gained by studying the critical manifold and its stability. This analysis can be split into three cases: all lasers are off, all lasers are on, or only a subpopulation is on. From Eq. (4), we have that $\dot{X} = 0 \Leftrightarrow X = \frac{1}{N}\sum_{i=1}^{N} x_i y_i$. The critical manifold is a solution of $\Delta - Y + kw + kf(X) - X = 0$, reminiscent of the case $N = 1$. It is clear that $\dot{X} = 0$ is satisfied either if all lasers are

off: $x_i = 0 \ \forall i$, which gives $Y_w = \Delta + kw$; or if all lasers are on: $y_i = 1 \ \forall i$, so that $Y = 1$. This provides two of the one-dimensional branches of the critical manifold of the full network. These curves are defined by exactly the same equations as for the case $N = 1$ but where all the variables and parameters are replaced by their corresponding mean values.

To analyze the critical manifold S in the general case, we parametrize it by the set I of switched-ON lasers and we introduce the new variable $X_I = \frac{1}{N} \sum_{i \in I} x_i$ and the parameter $\Delta_I = \frac{1}{N} \sum_{i \in I} \delta_i$. We find that

$$S_I = \left\{ \left(x_i^I(w), y_i^I(w), w \right), \ i = 1 \ldots N, \ w \in \mathbb{R} \right\},$$

with

$$\left(x_i^I(w), y_i^I(w) \right) = \begin{cases} (0, \delta_i + k[w + f(X_I(w))]), & \forall i \notin I, \\ (\delta_i - 1 + k[w + f(X_I(w))], 1) & \forall i \in I, \end{cases}$$

where $X_I(w)$ is implicitly defined by

$$X_I(w) = \frac{N_+}{N} (k[w + f(X_I(w))] - 1) + \Delta_I. \quad (7)$$

The critical manifold S of the coupled network thus consists of 2^N components: $S = \cup_{I \subset [1,N]} S_I$. Apart from the scaling factor $\frac{N_+}{N}$, the structure of the critical manifold is a bundle of one-dimensional branches S_I which, at zero order in z, closely resembles that of the $N = 1$ case except for the "off" nodes, those for which $x_i = 0$. The stability of S_I can be determined analytically assuming that all lasers are similar enough, $\delta_i = \Delta + z\eta_i, z \ll 1$. The calculations are not immediate (they are detailed in Appendix C) but demonstrate that the stability of S_I is, at zero order z, very similar to that of a single "mean" laser with control parameter Δ. However, nodes which would remain on the "off" branch without coupling may be expelled from it by the coupling through w.

Thus, as the quenched disorder δ_i is not averaged in the limit $N \to \infty$, a truly mean-field limit cannot be established as an ODE. However, due to the splitting of the timescales, most of the motion takes place along the critical manifold, leading to an effective low-dimensional dynamics similar to that of a single element. In Fig. 4 we plot the numerical mean-field trajectory together with the critical manifold of an average laser. The slow evolution of different nodes is perfectly synchronized, even if some elements may be on different branches of the slow manifold [explaining the experimental observation Fig. 1(d)]. However, the individual trajectories differ in the fast dynamics, transverse to the slow manifold. This is clear on the right of Fig. 4, which shows a time trace of the mean field together with the variance of the x_i. In absence of noise, the distribution of the x_i tends to a Dirac function whenever the system is close to the critical manifold, with a much broader distribution when the system switches branch. It is worth noting that the different trajectories persist even when the timescales differ by several orders of magnitude, as we have checked up to $\gamma = 4 \times 10^{-3}, \epsilon = 10^{-7}$.

Finally, the dynamics for $z \ll 1, N < \infty$ stays in a tube around the dynamics for $z = 0$, in which case there is no disorder and thus the dynamics is exactly that of the isolated laser. This implies that the MMO and the chaotic behaviors (for $z = 0$) are robust on finite time intervals when N grows to
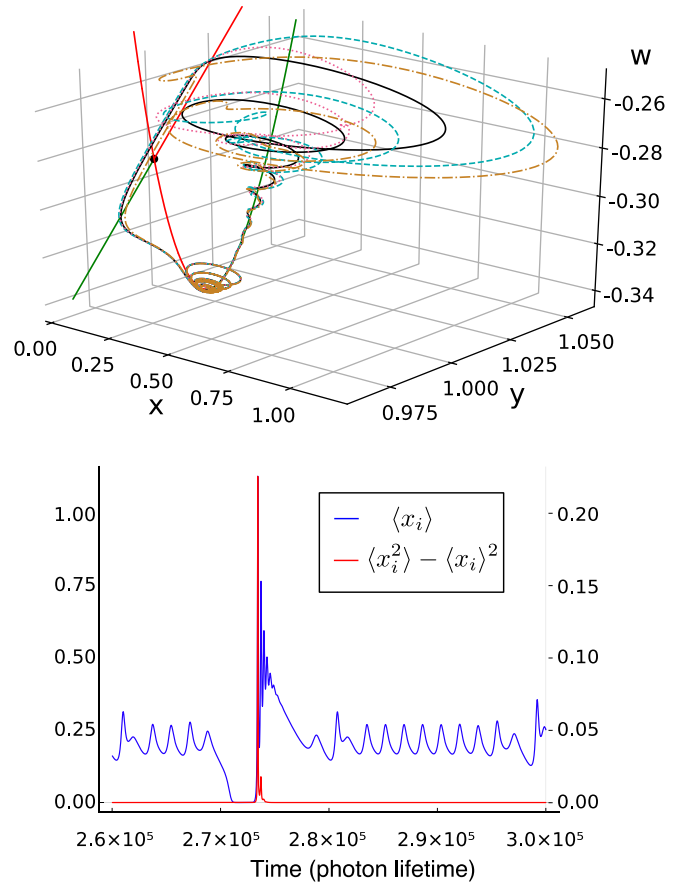

FIG. 4. Numerical simulations of 10^4 coupled lasers modeled by (1). Only three laser dynamics are plotted (dashed and dotted lines). The mean dynamics is plotted in continuous black. The parameters $\frac{\delta_i - \langle \delta \rangle}{\langle \delta \rangle}$ are independent Gaussian variables of zero mean and standard deviation 1×10^{-3} with $\langle \delta \rangle = 1.2045, k = 0.7, A = 1, \alpha = 2, \gamma = 4 \times 10^{-3}, \epsilon = 10^{-4}$. Black dot: intersection between the two slow manifold branches. The parabola Σ_y and the straight line Σ_x constitute the critical manifold calculated for a single laser with parameter Δ.

infinity. As an example, Fig. 4 shows a chaotic trajectory with $z \ll 1, N = 10^4$.

IV. EXPERIMENTAL VALIDATION

One theoretical prediction from the above is that the average threshold parameter Δ rules the dynamics. We corroborate this experimentally by measuring the total intensity for different population sizes (Fig. 5). All parameters are constant and the iris is opened to include a larger and larger population. For each network size, the total amount of light sent to the reinjection detector is scaled to keep the coupling parameter constant. We show the bifurcation diagrams of networks of 19 (D), 251 (E), and 451 (F) nodes on Fig. 5. Similar sequences are observed, although for different values of the control parameter. The distributions of the uncoupled laser emission thresholds are shown on the right column. The 451- and 251-element networks are very similar, but the 19-element one differs markedly. As expected from theory, this hints at Δ as the control parameter for the network.
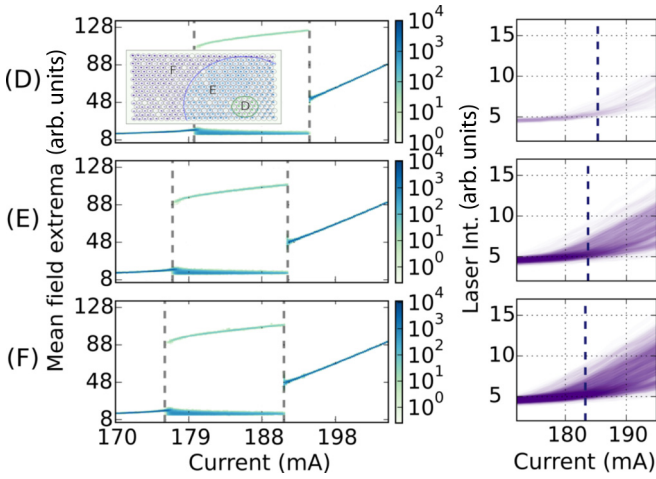
FIG. 5. Bifurcation diagrams of three networks of different sizes (D:19, $\langle I_{th} \rangle = 185.32$ mA; E:251$\langle I_{th} \rangle = 183.70$ mA; F:451). Right: bifurcation curves for the uncoupled elements, and the dashed line indicates $\langle I_{th} \rangle$.

We demonstrate this by measuring the current value at which some prescribed dynamics takes place for different populations. In Fig. 6 we plot the current value $\mathcal{I}_s$ at which the network returns to a stable fixed point after undergoing the sequence of bifurcations described earlier, as a function of the average threshold current of the subpopulation. The size and color of each marker indicate the size of the network. The error bars are estimates of the measurement error. Smaller networks are disperse, but larger networks converge towards the same point in this ($\langle I_{th} \rangle$, $\mathcal{I}_s$) space. The dispersion of the measurements around a straight line results from the scaling of the bifurcation parameter $\Delta = \frac{I_0 - I_t}{\langle I_{th} \rangle - I_t}$, where I_t is the transparency current (assumed to be equal for all devices).

V. CONCLUSION

Summarizing, we have observed experimentally collective mixed mode oscillations and spiking in a mean-field coupled network of hundreds of lasers. The results are robust with respect to some disorder (couplings or individual laser impedances). Of course, many details are not taken into account by the model, such as electronic characteristics of the
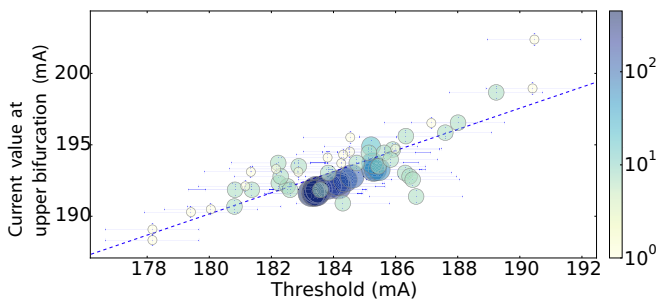

FIG. 6. Upper bifurcation parameter value depending on average laser threshold value for increasing sample size. Smaller samples (lighter blue) are distributed along a straight line. When the sample grows (darker blue) the bifurcation parameter converges to a well-defined value.

individual lasers, which may result in additional intermediate timescales. However, this does not alter the key dynamical scenario, and we expect that our results open several research avenues on the role of noise in coupled slow-fast systems and on networks of networks. More importantly, we significantly reduce the gap between the numerous existing predictions of collective spiking and the very scarce laboratory experiments. A transport equation for the probability density $p(t, x, y, w, \delta)$ of the limit laser when $N \longrightarrow \infty$ involves the full distribution of δ_i, which shows that the mean field cannot be described with an ODE. However, through the stability analysis of the critical manifold, we demonstrate that the network experiences an effectively low-dimensional dynamics, even when the fast dynamics of the nodes is not synchronized. Thus, we have presented a scenario leading to effectively low-dimensional dynamics of a large network. Since the analytics are model specific, the theory is hard to generalize formally and we leave that for future work. However, we believe that many slow-fast systems coupled in mean field through their slowest variable could follow the same scenario.

APPENDIX A: LASER ARRAY BASIC CHARACTERIZATION

In the main text we provide mean value and standard deviation of the threshold current of the lasers. Here for completeness we show the experimentally measured threshold current distribution on Fig. 7.

The lasers couple only incoherently on the photodetector due to their spectral distribution, which spans approximately 2 nm. An incoherent sum is shown in Fig. 8, where we show a far field image of the whole array. No signs of interference are detected, which indicates an incoherent sum.
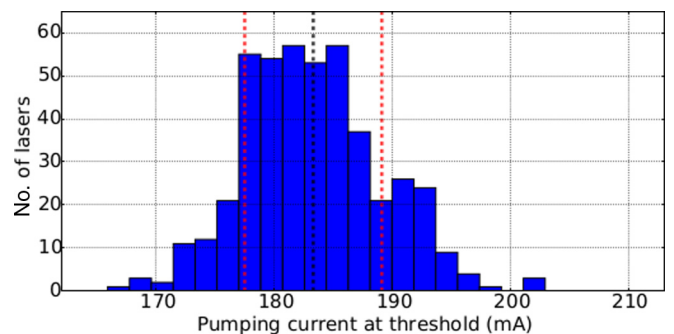

FIG. 7. Distribution of laser threshold currents. The vertical lines are the average and standard deviation of the distribution.
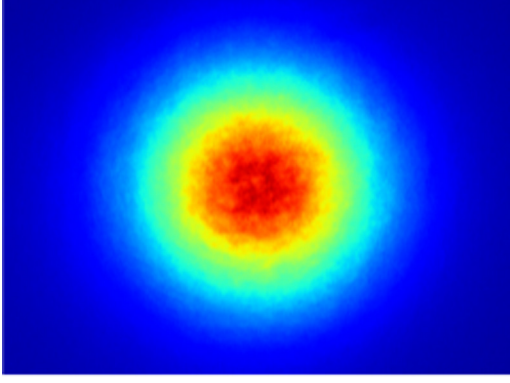
FIG. 8. Far field image showing incoherent superposition of the 451 laser intensities.

APPENDIX B: MODEL DETAILS

The single laser with optoelectronic feedback can be modeled with the following system:

$$\dot{s} = [g(n - n_t) - \gamma_0]s, \tag{B1}$$

$$\dot{n} = \frac{I_0 + kI}{ev} - \gamma_c n - g(n - n_t)s, \tag{B2}$$

$$\dot{I} = -\gamma_f I + f_f(\dot{s}). \tag{B3}$$

After proper scaling, $x = \frac{g}{\gamma_c s}$, $y = \frac{g}{\gamma_0}(n - n_t)$, and $w = I - f_f(\frac{\gamma_c}{g} x)$, we end up with the following system for a fully connected network for $i = 1, \dots, N$:

$$\dot{x}_i = x_i(y_i - 1), \tag{B4}$$

$$\dot{y}_i = \gamma[\delta_i - y_i + k(w + f(X)) - x_i y_i], \tag{B5}$$

$$\dot{w} = -\epsilon(w + f(X)), \tag{B6}$$

where the time variable has been normalized to the photon lifetime and x_i, y_i are respectively the dimensionless photon and carrier density of the laser i. $X = \frac{1}{N}\sum_{i=1}^{N} x_i$ is the total intensity normalized to the number of elements in the network. The global variable w is the (scaled) high-pass filtered feedback current, which includes a saturable nonlinear function $f(X) = A \ln(1 + \alpha X)$.

APPENDIX C: EQUILIBRIA AND CRITICAL MANIFOLD STABILITY

Throughout this section, I denotes a subset of the integers $[1, N]$ of the cardinal N_+. It will be used to label the lasers which are switched ON.

1. Stationary states

We start by computing the stationary solutions of (B4) when N lasers are connected. Let us write P_I the equilibrium for which $\forall i \in I, x_i > 0$ and $x_i = 0$ otherwise. One also can define $X_I^{eq} = \frac{1}{N}\sum_{i \in I} x_i$. We first have $0 = w + f(X_I^{eq})$.
(1) Case $i \in I$. One finds that $x_i = \delta_i - 1$ and $y_i = 1$.
(2) Case $i \notin I$. It gives $x_i = 0$ and $y_i = \delta_i$.

Finally, $w = -f(\frac{1}{N}\sum_{i \in I}\delta_i - \frac{N_+}{N})$. Note that there are 2^N such equilibria.

a. Stability of the stationary states

In this section, we compute the stability of the equilibria P_I. To this end, we write $x_i(t) = x_i^{eq} + e^{\lambda t} u_i$, $y_i(t) = y_i^{eq} + e^{\lambda t} v_i$, and $w(t) = w^{eq} + e^{\lambda t}\omega$. We then Taylor expand (B4)–(B6) under the assumption that u_i, v_i, ω are small. The goal is to find the eigenvalues λ associated to a nontrivial set of u_i, v_i, ω. One gets $X_I^{eq} := \frac{1}{N}\sum_i x_i^{eq}$, and

$$\lambda u_i = x_i^{eq} v_i + u_i(y_i^{eq} - 1),$$

$$\lambda v_i = \gamma\left\{-v_i - x_i^{eq} v_i - u_i y_i^{eq} + k\left[\omega + f'(X_I^{eq})\frac{1}{N}\sum_k u_k\right]\right\},$$

$$\lambda\omega = -\epsilon\left[\omega + f'(X_I^{eq})\frac{1}{N}\sum_k u_k\right],$$

which gives

$$(\lambda - y_i^{eq} + 1)u_i = x_i^{eq} v_i, \tag{C1}$$

$$(\lambda + \gamma + \gamma x_i^{eq})v_i = -\gamma u_i y_i^{eq} - \gamma k\frac{\lambda}{\epsilon}\omega, \tag{C2}$$

$$(\lambda + \epsilon)\omega = -\epsilon f'(X_I^{eq})\frac{1}{N}\sum_k u_k. \tag{C3}$$

We can find some eigenvalues analytically. Indeed, if we consider $i_0 \notin I$, then $x_{i_0}^{eq} = 0$. This gives the following cases:

(1) Case $u_{i_0} = 1$. We find that $\lambda = y_{i_0}^{eq} - 1$ is an eigenvalue. Indeed, set $u_i = v_i = 0$ for $i \neq i_0$. Then $\omega = -\frac{1}{N}\frac{\epsilon}{\lambda + \epsilon}f'(X^{eq})$, and v_{i_0} is found using Eq. (C2). This gives $N - N_+$ eigenvalues.

(2) Case $u_{i_0} = 0$. We find that $\lambda = -\gamma$ is an eigenvalue. Indeed, set $u_i = v_i = 0$ for $i \neq i_0$. Then $\omega = 0$, and $v_{i_0} = 1$ is a solution of the above equations. This gives $N - N_+$ eigenvalues.

We now look for the remaining eigenvalues. Using the above Eqs. (C1)–(C3), one finds

$$\left(\lambda - y_i^{eq} + 1 + \frac{\gamma x_i^{eq} y_i^{eq}}{\lambda + \gamma + \gamma x_i^{eq}}\right)u_i$$

$$= \frac{x_i^{eq}}{\lambda + \gamma + \gamma x_i^{eq}}\frac{\lambda}{\lambda + \epsilon}\left[\frac{\tilde{A}_I}{N}\sum_k u_k\right],$$

where we wrote $\tilde{A}_I := \gamma k f'(X_I^{eq})$. By summing this equation w.r.t. i, one extracts an equation for $\sum_i u_i \neq 0$ and get

$$1 = \frac{\tilde{A}_I}{N}\frac{\lambda}{\lambda + \epsilon}\sum_{i=1}^{N}\frac{x_i^{eq}}{\gamma x_i^{eq} y_i^{eq} + (\lambda + \gamma + \gamma x_i^{eq})(\lambda - y_i^{eq} + 1)}.$$

We can simplify this equation in the case of the equilibrium P_I when $\lambda + \gamma \neq 0$ and $\lambda \neq \delta_i - 1$ for $i \notin I$ into an equation accounting for the dynamics of the switched-ON lasers:

$$1 = \frac{\tilde{A}_I}{N}\frac{\lambda}{\lambda + \epsilon}\sum_{i \in I}\frac{x_i^{eq}}{\gamma x_i^{eq} + \lambda(\lambda + \gamma + \gamma x_i^{eq})}. \tag{C4}$$

Note that this polynomial equation has at most $2N_+ + 1$ zeros, which in addition to the other $2(N - N_+)$ zeros, gives $2N + 1$ eigenvalues as expected.

b. Approximation of small deviation

Solving the previous Eq. (C4) is tedious, but we can simplify it. Let us assume that $\delta_i = \Delta + z\eta_i$, where $z \ll 1$, i.e., the control parameters are peaked at around Δ. We use the fact that $x_i^{eq} = \Delta - 1 + z\eta_i$ for $i \in I$ and rewrite (C4) as $1 = P(\lambda, z)$. Also, we write $\tilde{A}_I = \tilde{A}_I^0 + z\tilde{A}_I^1 = \gamma k f'[\frac{N_+}{N}(\Delta - 1)] + z\gamma k f''[\frac{N_+}{N}(\Delta - 1)]\frac{1}{N}\sum_{i \in I}\eta_i$.

Using Maple, we Taylor expand $P(\lambda, z)$ in z at first order:

$$1 = \frac{1}{N}\frac{\lambda}{\lambda + \epsilon}$$
$$\times \left((\tilde{A}_I^0 + z\tilde{A}_I^1)N_+ \frac{\Delta - 1}{\gamma(\Delta - 1) + \lambda[\lambda + \gamma + \gamma(\Delta - 1)]} \right.$$
$$\left. + z \frac{\tilde{A}_I^0\lambda(\lambda + \gamma)}{\{\gamma(\Delta - 1) + \lambda[\lambda + \gamma + \gamma(\Delta - 1)]\}^2}\sum_{i \in I}\eta_i \right).$$

We solve this equation perturbatively by seeking $\lambda = \lambda_0 + z\lambda_1 + O(z^2)$. One gets

$$1 = \tilde{A}_I^0 \frac{N_+}{N}\frac{\lambda_0}{\lambda_0 + \epsilon}\frac{\Delta - 1}{\gamma(\Delta - 1) + \lambda_0[\lambda_0 + \gamma + \gamma(\Delta - 1)]}$$

and

$$\lambda_1 \propto \sum_{i \in I}\eta_i.$$

The first equation in λ_0 is solved similarly to the single-laser case. When $N_+ = N$ (all lasers are ON), the x_i^{eq} solve the same equations as for the isolated laser with common control parameter Δ.

If we chose $\Delta = \frac{1}{N}\sum_{i=1}^{N}\delta_i$, then one finds that $\frac{1}{N}\sum_{i=1}^{N}\eta_i = 0$, and thus λ_0 is precise at second order in z. The second-order correction to λ is then a function of the second moment $\sum_{i \in I}\eta_i^2$.

2. Critical manifold S_I

The critical manifold is defined by solving for each w the following equations:

$$0 = x_i(y_i - 1), \tag{C5}$$

$$0 = \gamma[\delta_i - y_i + k(w + f(X)) - x_i y_i]. \tag{C6}$$

As before, we parametrize the critical manifold by the set I, which labels the switched ON lasers. We denote by S_I the associated critical manifold. Note that the critical manifold is composed of 2^N components, namely, $S = \cup_{I \subset [1,N]} S_I$. Using the same arguments as for the equilibria, it is straightforward to show that

$$S_I = \{ [x_i^I(w), y_i^I(w), w], \ i = 1 \ldots N, \ w \in \mathbb{R} \},$$

with

$$[x_i^I(w), y_i^I(w)] = \begin{cases} \{0, \delta_i + k[w + f(X_I(w))]\}, & \forall i \notin I, \\ \{\delta_i - 1 + k[w + f(X_I(w))], 1\} & \forall i \in I, \end{cases}$$

where $X_I(w)$ is implicitly defined by

$$X_I(w) = \frac{N_+}{N}\{k[w + f(X_I(w))] - 1\} + \frac{1}{N}\sum_{i \in I}\delta_i. \tag{C7}$$

a. Stability of the critical manifold

In this section, we compute the eigenvalues of the linearized equation around the critical manifold when $\epsilon = 0$:

$$\dot{x}_i = x_i(y_i - 1), \tag{C8}$$

$$\dot{y}_i = \gamma[\delta_i - y_i + k(w + f(X)) - x_i y_i]. \tag{C9}$$

To this end, we write $x_i(t) = x_i^I(w) + e^{\lambda t}u_i$ and $y_i(t) = y_i^I(w) + e^{\lambda t}v_i$ and Taylor expand the above equation with the assumption that u_i, v_i are small. The goal is to find λ associated to a nontrivial set of u_i, v_i. One then gets

$$\lambda u_i = x_i^I v_i + u_i(y_i^I - 1),$$

$$\lambda v_i = \gamma\left[-v_i - x_i^I v_i - u_i y_i^I + k f'(X_I(w))\frac{1}{N}\sum_k u_k\right],$$

which gives

$$(\lambda - y_i^I + 1)u_i = x_i^I v_i \tag{C10}$$

$$(\lambda + \gamma + \gamma x_i^I)v_i = -\gamma u_i y_i^I + \gamma k f'(X_I(w))\frac{1}{N}\sum_k u_k \tag{C11}$$

We can find some eigenvalues analytically. Indeed, if we consider $i_0 \notin I$, then $x_{i_0}^I(w) = 0$. This gives the following cases:

(1) Case $u_{i_0} = 1$. We find that $\lambda = y_{i_0}^I(w) - 1$ is an eigenvalue. Indeed, set $u_i = v_i = 0$ for $i \neq i_0$. Then v_{i_0} is found using Eq. (C10). This gives $N - N_+$ eigenvalues.

(2) Case $u_{i_0} = 0$. We find that $\lambda = -\gamma$ is an eigenvalue. Indeed, set $u_i = v_i = 0$ for $i \neq i_0$. Then $v_{i_0} = 1$ is a solution of the above equation. This gives $N - N_+$ eigenvalues.

We now look for the remaining eigenvalues. Using the above Eqs. (C10) and (C11), one finds

$$\left(\lambda - y_i^I + 1 + \frac{\gamma x_i^I y_i^I}{\lambda + \gamma + \gamma x_i^I}\right)u_i$$
$$= \frac{x_i^I}{\lambda + \gamma + \gamma x_i^I}\left[\frac{\tilde{A}_I(w)}{N}\sum_k u_k\right],$$

where we wrote $\tilde{A}_I(w) := \gamma k f'(X_I(w))$. By summing this previous equation w.r.t. i, one extracts an equation for $\sum_i u_i \neq 0$:

$$1 = \frac{\tilde{A}_I(w)}{N}\sum_{i=1}^{N}\frac{x_i^I(w)}{\gamma x_i^I(w)y_i^I(w) + (\lambda + \gamma + \gamma x_i^I(w))(\lambda - y_i^I(w) + 1)}.$$

We can simplify this equation because (x_i^I, y_i^I) belongs to S_I, and when $\lambda + \gamma \neq 0$, $\lambda \neq y_i^I(w) - 1$ (for $i \notin I$):

$$1 = \frac{\tilde{A}_I(w)}{N} \sum_{i \in I} \frac{x_i(w)}{\gamma x_i(w) + \lambda(\lambda + \gamma + \gamma x_i(w))}. \quad (C12)$$

This provides an equation for the remaining $2N_+$ eigenvalues.

b. Small deviation approximation of the critical manifold

For notation purposes, we write $x_i^I(w) = x_i(w)$ and $y_i^I(w) = y_i(w)$.

Solving the previous Eq. (C12) is tedious but we can simplify it. Let us assume that $\delta_i = \Delta + z\eta_i$ where $z \ll 1$, i.e., the current values are peaked at around Δ. Our goal is to Taylor expand (C12) in z and solve it perturbatively. Hence, we need to find $x_i^I(w)$, $y_i^I(w)$ as a function of z.

We write $\forall i \in I$, $x_i(w) = x_i^0(w) + z x_i^1(w) + O(z^2)$ and note that $y_i(w) = 1$. To find these expressions, we need to find the following expressions: $X_I(w) = X_I^0(w) + z X_I^1(w) + O(z^2)$. We would then have $x_i^0(w) = \Delta - 1 + k[w + f(X_I^0(w))]$, which is independent of i and so is written $x_I^0(w)$, and $x_i^1(w) = \eta_i + k f'(X_I^0) X_I^1$. Using (C7), we find that $X_I^0(w)$, $X_I^1(w)$ solves

$$X_I^0(w) = \frac{N_+}{N}\{k[w + f(X_I^0(w))] - 1\} + \Delta,$$

and

$$X_I^1(w) = \frac{N_+}{N} k f'(X_I^0(w)) X_I^1 + \frac{1}{N} \sum_I \eta_i \Rightarrow X_I^1(w)$$

$$= \frac{\frac{1}{N}\sum_I \eta_i}{1 - \frac{N_+}{N} k f'(X_I^0(w))}.$$

We obtain the following expression:

$$x_i^1(w) = \eta_i + \frac{k f'(X_I^0(w))}{1 - \frac{N_+}{N} k f'(X_I^0(w))} \frac{1}{N} \sum_I \eta_i.$$

Note that the equation for x_I^0 is exactly the same equation as for the single laser but with parameters α, δ changed into $\alpha \frac{N_+}{N}$ and Δ.

c. Small deviation approximation of the stability of the critical manifold

We now proceed to find the stability of the critical manifold using (C12). As before, we write $\tilde{A}_I(w) = \tilde{A}_I^0(w) + z\tilde{A}_I^1(w) = \gamma k f'(X_I^0(w)) + z\gamma k f''(X_I^0(w)) X_I^1(w)$. We Taylor expand (C12) in z and find

$$1 = (\tilde{A}_I^0(w) + z\tilde{A}_I^1(w)) \frac{N_+}{N} \frac{x_I^0(w)}{\gamma x_I^0(w) + \lambda(\lambda + \gamma + \gamma x_I^0(w))}$$

$$+ z \frac{\lambda(\lambda + \gamma)}{[\gamma x_I^0(w) + \lambda(\lambda + \gamma + \gamma x_I^0(w))]^2} \frac{\tilde{A}_I^0(w)}{N} \sum_{i \in I} x_i^1(w).$$

We solve this equation perturbatively by seeking $\lambda = \lambda_0 + z\lambda_1 + o(z)$. One gets

$$1 = \tilde{A}_I^0(w) \frac{N_+}{N} \frac{x_I^0(w)}{\gamma x_I^0(w) + \lambda_0(\lambda_0 + \gamma + \gamma x_I^0(w))} \quad (C13)$$

and

$$\lambda_1 \propto \sum_{i \in I} \eta_i.$$

The first equation in λ_0 is quadratic and easily solved. In the case $N_+ = N$, as $x_I^0(w)$ solves the same equations as for the isolated laser, and one finds that λ_0 solves the same equation for the stability of the critical manifold. In effect, those two terms correspond to the single-laser case.

At zero order in z, the components $(x_i(w), y_i(w))$ for $i \in I$ of the critical manifold S_I are all the same and share the expression of the critical manifold (with $x > 0$) of the single laser with control parameter Δ and $\alpha \to \alpha \frac{N_+}{N}$. When $N_+ = N$ and at zero order in z, the stability of the $S_{[1,N]}$ branch is therefore the same as that of an uncoupled laser with control parameter Δ. However, when $N_+ < N$, the other eigenvalues $y_i(w) - 1$ may influence the stability of S_I.

d. Summary

The above discussion hints at introducing the laser dynamics

$$\dot{x} = x(y - 1), \quad (C14)$$

$$\dot{y} = \gamma\left\{\Delta - y + k\left[w + f\left(\frac{N_+}{N}x\right)\right] - xy\right\}, \quad (C15)$$

$$\dot{w} = -\epsilon\left[w + f\left(\frac{N_+}{N}x\right)\right], \quad (C16)$$

with the critical manifold composed of the OFF branch $(0, \Delta + kw)$ and the ON branch $(x^{\text{crit}}, 1)$, where x^{crit} solves

$$x^{\text{crit}}(w) = \Delta - 1 + k\left[w + f\left(\frac{N_+}{N}x^{\text{crit}}(w)\right)\right].$$

The eigenvalues along the OFF branch are $\Delta + kw - 1$ and $-\gamma$. The eigenvalues λ along the ON branch are solutions of

$$\lambda(\lambda + \gamma + \gamma x^{\text{crit}}(w)) - \gamma\left[k\frac{N_+}{N}f'\left(\frac{N_+}{N}x^{\text{crit}}(w)\right) - 1\right]x^{\text{crit}}$$

$$= 0. \quad (C17)$$

At zeroth order in z, the critical manifold S_I is given by $(x_i^I(w), y_i^I(w)) = [0, \Delta + kw + kf(\frac{N_+}{N}x^{\text{crit}}(w))]$ for $i \notin I$ and $(x_i^I(w), y_i^I(w)) = (x^{\text{crit}}(w), 1)$ for $i \in I$. Hence, only the OFF part of the critical manifold S_I differs from the above model with the correction shown in red. For the stability of S_I, we have the eigenvalues $-\gamma$, $\Delta + kw + kf(\frac{N_+}{N}x^{\text{crit}}(w)) - 1$ and the solutions of (C17) [which are the same as those of (C13)]. Hence, only the OFF part of the dynamics is inadequately described by (C14)–(C16).

[1] Z. Néda, E. Ravasz, T. Vicsek, Y. Brechet, and A.-L. Barabási, Phys. Rev. E **61**, 6987 (2000).

[2] Y. Kuramoto, *Chemical Oscillations, Waves, and Turbulence* (Springer Science & Business Media, New York, 2012), Vol. 19.

[3] S. H. Strogatz, Phys. D (Amsterdam, Neth.) **143**, 1 (2000).

[4] P. Jiruska, M. De Curtis, J. G. Jefferys, C. A. Schevon, S. J. Schiff, and K. Schindler, J. Phys. **591**, 787 (2013).

[5] R. E. Mirollo and S. H. Strogatz, SIAM J. Appl. Math. **50**, 1645 (1990).

[6] S. Watanabe and S. H. Strogatz, Phys. D (Amsterdam, Neth.) **74**, 197 (1994).

[7] R. Zillmer, R. Livi, A. Politi, and A. Torcini, Phys. Rev. E **74**, 036203 (2006).

[8] S. Olmi, A. Navas, S. Boccaletti, and A. Torcini, Phys. Rev. E **90**, 042905 (2014).

[9] K. Kotani, I. Yamaguchi, L. Yoshida, Y. Jimbo, and G. B. Ermentrout, J. R. Soc. Interface **11**, 20140058 (2014).

[10] E. Montbrió, D. Pazó, and A. Roxin, Phys. Rev. X **5**, 021028 (2015).

[11] D. Pazó and E. Montbrió, Phys. Rev. Lett. **116**, 238101 (2016).

[12] E. Ott and T. M. Antonsen, Chaos: An Int. J. Nonlinear Sci. **18**, 037113 (2008).

[13] E. Ott and T. M. Antonsen, Chaos: An Interdisciplinary J. Nonlinear Sci. **19**, 023117 (2009).

[14] M. Nixon, M. Friedman, E. Ronen, A. A. Friesem, N. Davidson, and I. Kanter, Phys. Rev. Lett. **106**, 223901 (2011).

[15] M. Nixon, M. Fridman, E. Ronen, A. A. Friesem, N. Davidson, and I. Kanter, Phys. Rev. Lett. **108**, 214101 (2012).

[16] F. Selmi, R. Braive, G. Beaudoin, I. Sagnes, R. Kuszelewicz, and S. Barbay, Phys. Rev. Lett. **112**, 183902 (2014).

[17] A. Hurtado and J. Javaloyes, Appl. Phys. Lett. **107**, 241103 (2015).

[18] T. Sorrentino, C. Quintero-Quiroz, A. Aragoneses, M. Torrent, and C. Masoller, Opt. Express **23**, 5571 (2015).

[19] C. Mesaritakis, A. Kapsalis, A. Bogris, and D. Syvridis, Sci. Rep. **6**, 39317 (2016).

[20] P. R. Prucnal, B. J. Shastri, T. F. de Lima, M. A. Nahmias, and A. N. Tait, Adv. Opt. Photonics **8**, 228 (2016).

[21] A. Dolcemascolo, B. Garbin, B. Peyce, R. Veltz, and S. Barland, Phys. Rev. E **98**, 062211 (2018).

[22] B. Garbin, J. Javaloyes, G. Tissoni, and S. Barland, Nat. Commun. **6**, 5915 (2015).

[23] B. Romeira, R. Avó, J. M. Figueiredo, S. Barland, and J. Javaloyes, Sci. Rep. **6**, 19510 (2016).

[24] S. Terrien, B. Krauskopf, N. G. Broderick, R. Braive, G. Beaudoin, I. Sagnes, and S. Barbay, Optics Lett. **43**, 3013 (2018).

[25] A. M. Yacomotti, G. B. Mindlin, M. Giudici, S. Balle, S. Barland, and J. Tredicce, Phys. Rev. E **66**, 036227 (2002).

[26] B. Kelleher, C. Bonatto, P. Skoda, S. Hegarty, and G. Huyet, Phys. Rev. E **81**, 036204 (2010).

[27] T. Van Vaerenbergh, M. Fiers, P. Mechet, T. Spuesens, R. Kumar, G. Morthier, B. Schrauwen, J. Dambre, and P. Bienstman, Opt. Express **20**, 20292 (2012).

[28] T. Deng, J. Robertson, and A. Hurtado, IEEE J. Sel. Top. Quantum Electron. **23**, 1800408 (2017).

[29] S. Abdalah, K. A. Naimee, M. Ciszak, F. Marino, R. Meucci, and F. Arecchi, Acta Phys. Pol. A **121**, 7 (2012).

[30] I. Belykh, E. de Lange, and M. Hasler, Phys. Rev. Lett. **94**, 188101 (2005).

[31] K. Al-Naimee, F. Marino, M. Ciszak, R. Meucci, and F. T. Arecchi, New J. Phys. **11**, 073022 (2009).

[32] F. Marino, M. Ciszak, S. F. Abdalah, K. Al-Naimee, R. Meucci, and F. T. Arecchi, Phys. Rev. E **84**, 047201 (2011).

[33] N. Fenichel, J. Differ. Equations **31**, 53 (1979).

[34] N. Berglund and B. Gentz, *Noise-Induced Phenomena in Slow-Fast Dynamical Systems: A Sample-Paths Approach*, edited by N. Berglund and B. Gentz, Probability and Its Applications (Springer Science & Business Media, New York, 2006).

[35] K. Al-Naimee, F. Marino, M. Ciszak, S. Abdalah, R. Meucci, and F. Arecchi, Eur. Phys. J. D **58**, 187 (2010).

[36] C. Rackauckas and Q. Nie, J. Open Res. Software **5**, 15 (2017).